Supplementary Information

One-pot lignocellulosic bioplastics synthesis through in-situ deconstruction of deep eutectic solvent

Wang Zhao‡ *Jianbo Shuai*‡ *Hao Hu* *Nuo Xu* *Cheng Xu* *Zepeng Lei** *Xiaohui Wang**

State Key Laboratory of Advanced Papermaking and Paper-based Materials, South China University of Technology, Guangzhou 510640, China

**Corresponding author*

Email address: zepenglei@scut.edu.cn (Z. Lei); fewangxh@scut.edu.cn (X. Wang)

‡ *These authors contributed equally to this work.*

This file includes:

1. Characterization Methods

1.1 Solvent Structure and Gas Composition Analysis

Nuclear Magnetic Resonance (NMR) Spectroscopy: Structural changes in the solvents were analyzed using a 500 MHz NMR spectrometer (Bruker, Germany). Samples were dissolved in DMSO-d6, and ^{1}H NMR spectra were acquired with 32 scans.

Viscosity: The shear viscosity of the solvents was measured using a rotational rheometer (NDJ-8S, LICHEN Tech., China) at temperatures ranging from 25 to 100 ℃ and a shear rate of 0.02 s^{-1}.

Thermal Stability: Thermogravimetric analysis (TGA) was performed on a Netzsch TG209F3 instrument (Germany) under nitrogen atmosphere. The temperature was raised from 40 to 600 ℃ at a rate of 10 ℃ min^{-1} to obtain TG and DTG curves.

Gas Composition: Gaseous products released from DBNACl/MeC-2/1 (30 g) heated at 150 ℃ in a sealed two-neck flask equipped with a balloon were collected and analyzed using gas chromatography–mass spectrometry (GC–MS, Agilent 6890N-5973) equipped with a WM-624 column (60 m × 320 μm × 1.8 μm).

1.2 Characterization of Bagasse Solutions

Rheological Properties: Shear viscosity of the solutions was determined at 25 ℃ with shear rates from 0.1 to 100 s^{-1} using a rotational rheometer (NDJ-8S, LICHEN Tech., China).

Transmittance: UV-Vis spectra (400–800 nm) were recorded on a Shimadzu UV-2600i spectrophotometer (Japan) with a step size of 0.5 nm to evaluate absorbance and transmittance.

1.3 Physicochemical Properties of Regenerated Bagasse

Regeneration Yield: The regeneration yield was calculated as the weight percentage of the dried regenerated residue relative to the initial mass of bagasse.

Compositional Analysis: Extractives were removed from raw and regenerated

bagasse using a benzene/ethanol mixture (2:1, v/v) following Chinese National Standard GB/T 2677.6-1994.

(1) Lignin Content: Acid-insoluble lignin was quantified according to GB/T 2677.8-1994. Extractives-free samples (1 g) were treated with 72% H_2SO_4 (15 mL) at 20 ℃ for 2.5 h, diluted to 3% H_2SO_4, refluxed for 4 h, and filtered. Acid-soluble lignin was determined spectrophotometrically following GB/T 10337-2008. Total lignin is reported as the sum of both fractions.

(2) Cellulose Content: The α-cellulose content was determined using the nitric acid-ethanol method. Samples (1 g) were refluxed three times with fresh nitric acid/ethanol (1:4, v/v; 25 mL each), and the insoluble residue was defined as α-cellulose.

(3) Hemicellulose Content: Holocellulose was isolated according to GB/T 2677.10-1995 by treating samples (2 g) with aqueous sodium chlorite (0.6 g, 80%) and acetic acid (0.5 mL) at 75 ℃ for three 1 h cycles. Hemicellulose content was calculated as the difference between holocellulose and α-cellulose.

Degree of Polymerization (DP): The viscosity of bagasse solutions in cupriethylenediamine (CED) was measured using an Ubbelohde viscometer according to GB/T 1548-2016.

FTIR Spectroscopy: Functional groups were analyzed using a Bruker VERTEX 70 FTIR spectrometer with KBr pellets. Spectra were collected over 4000–500 cm^{-1} at a resolution of 0.01 cm^{-1} with 32 scans per sample.

Crystallinity: X-ray diffraction (XRD) patterns were recorded on a PANalytical X'pert Powder diffractometer (Netherlands) with Cu Kα radiation (30 kV, 10 mA) over 5–60° (2θ) at 5° min^{-1}.

Surface Elemental Analysis: X-ray photoelectron spectroscopy (XPS) was performed on a Thermo Scientific K-Alpha Nexsa instrument (USA). Survey and high-resolution C 1s spectra were acquired, and atomic ratios (C/O) and carbon bond distributions were determined via peak integration.

1.4 Structural Characterization of Regenerated Lignin

Two-dimensional heteronuclear single quantum coherence (2D-HSQC) NMR spectra were acquired on a Bruker AVIII HD 500 MHz spectrometer (Germany). Lignin samples (~50 mg) were dissolved in 0.6 mL DMSO-d6. Spectra were recorded with spectral widths of 5000 Hz (^{1}H) and 20000 Hz (^{13}C), 1024 data points in the ^{1}H dimension, a recycle delay of 1.5 s, and 64–256 increments in the ^{13}C dimension. Chemical shifts were referenced to DMSO-d6 (δC/δH = 39.52/2.50). Volume integration of cross-signals was performed, and the relative abundances of lignin units (S, G, H) and inter-unit linkages (β–O–4, β–β, β–5) were semi-quantitatively calculated per 100 aromatic rings using established formulas:

$$TAR = 1/2(S2/6 + S'2/6) + 1/3(G2 + G5 + G6) + 1/2H2/6$$

$$S\% = \frac{(S2/6 + S'2/6)}{(2TAR)} \times 100\%$$

$$G\% = \frac{(G2 + G5 + G6)}{(3TAR)} \times 100\%$$

$$H\% = \frac{(H2/6)}{(2TAR)} \times 100\%$$

$$(\beta - O–4)\% = \frac{(\beta - O - 4'\alpha)}{(TAR)} \times 100\%$$

$$(\beta–\beta)\% = \frac{(\beta–\beta\alpha)}{(TAR)} \times 100\%$$

$$(\beta–5)\% = \frac{(\beta–5\alpha)}{(TAR)} \times 100\%$$

Where, TAR (Total Aromatic Ring count) is defined as the sum of aromatic rings. S%, G%, and H% represent the relative contents of S-, G-, and H-type units, respectively. The terms (β–O–4)%, (β–β)%, and (β–5)% denote the relative abundances of the β−O–4, β–β, and β–5 linkage types, respectively. $S_{2/6}$ and $S'_{2/6}$ correspond to the integrated signal areas for $C_{2/6}$ cross-linking in S- and S′-type units, respectively. G_2, G_5, and G_6 refer to the integrated signal areas for cross-linking at the C_2, C_5, and C_6 positions of G-type units, while $H_{2/6}$ represents the integrated signal area for $C_{2/6}$ cross-linking in H-type units.

1.5 Performance Evaluation of Regenerated Composites

Mechanical Properties: Tensile tests were conducted on an INSTRON 5565 universal testing machine (USA) at a crosshead speed of 10 mm min^{-1} with a 20 mm

gauge length. Five replicates were tested for each sample.

Optical Properties: Transmittance spectra (200–1000 nm) were recorded on a Shimadzu UV-2600i spectrophotometer (Japan). Haze was measured using a PerkinElmer Lambda950 spectrophotometer (USA) over 400–1000 nm.

Thermal Stability: Thermogravimetric analysis was performed on a NETZSCH TG 209 F1 Libra instrument under nitrogen (20 mL min^{-1}) from 40 to 600 ℃ at 10 ℃ min^{-1}.

Barrier Properties: The water vapor transmission rate (WVTR) was measured at 25 ℃ and 70% relative humidity using a W413 2.0 permeability tester.

Morphology and Elemental Mapping: Surface morphology was observed using a Hitachi SU5000 scanning electron microscope (Japan) after gold coating. Elemental distribution (C, O, N) was analyzed via energy-dispersive X-ray spectroscopy (EDS) on a Bruker GENESIS XM system (Germany).

2. Supplementary Figures and Tables

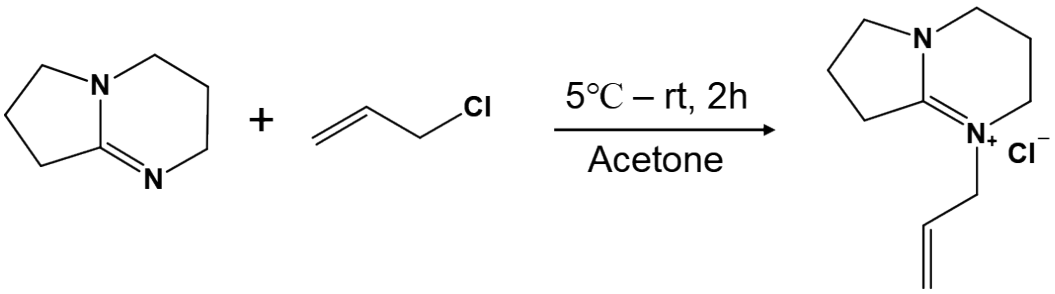

Fig. S1. Synthesis route of DBNACl.

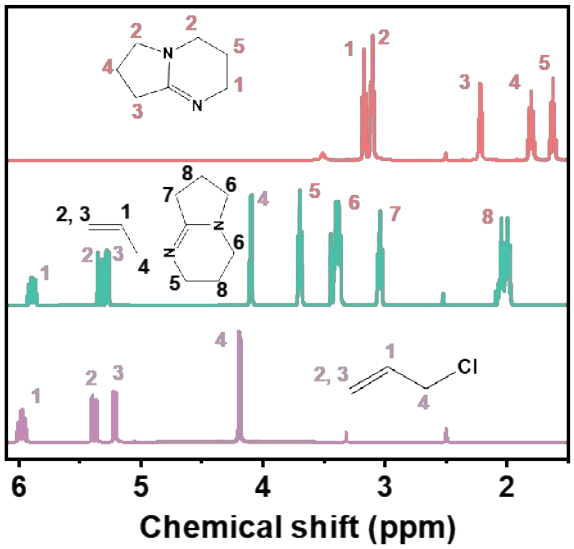

Fig. S2. ^{1}H NMR spectrum of DBNACl.

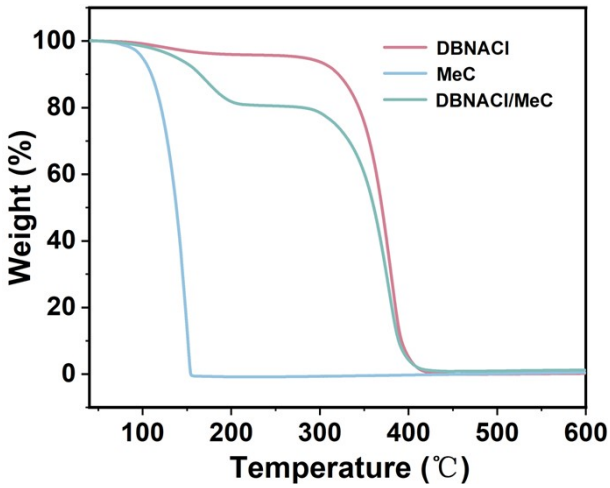

Fig. S3. TGA curves of DBNACl, MeC, and DBNACl/MeC-2/1.

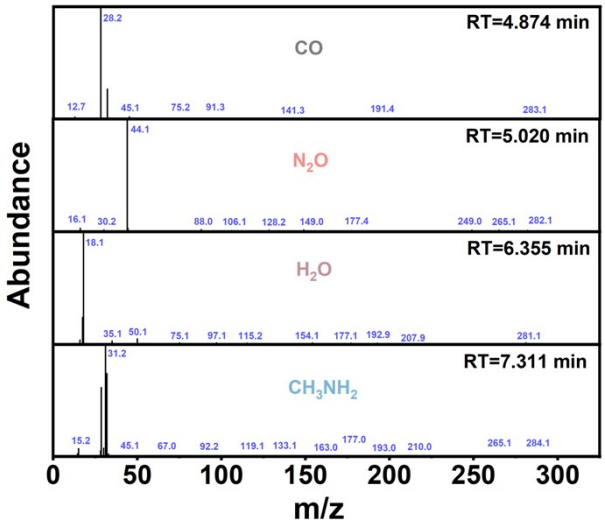

Fig. S4. MS spectra of gas component.

Table S1. Solubility of gas-generating SIL-DESs for MCC at 90℃.

Samples	HBA	HBDs	DESs formation	Solubility (wt%)	
				HBA:HBD=2/1	HBA:HBD=1/1
1	DBNACl	MeC	√	14.7	11
2		EtC	√	14.3	9.2
3		BuC	√	13.5	6.1
4		AcH	√	11.8	4.4
5		CaH	√	9.9	5.5
6		PhH	√	7.9	3.9
7		HyH	×	-	-

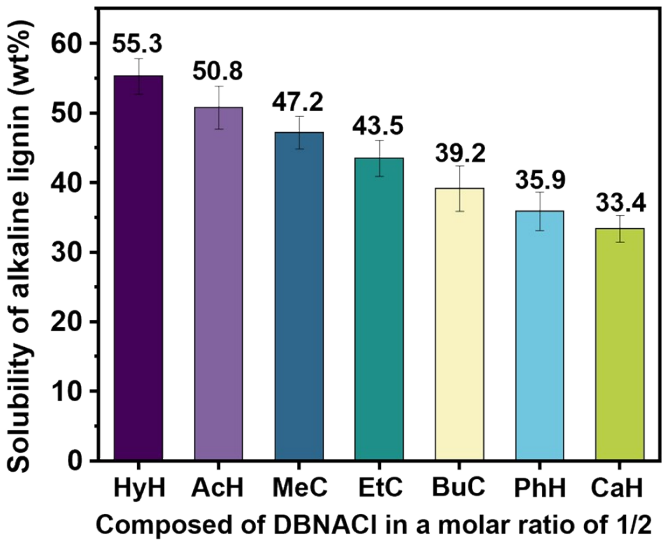

Fig. S5. Solubility of gas-generating SIL-DESs for alkaline lignin at 90 ℃.

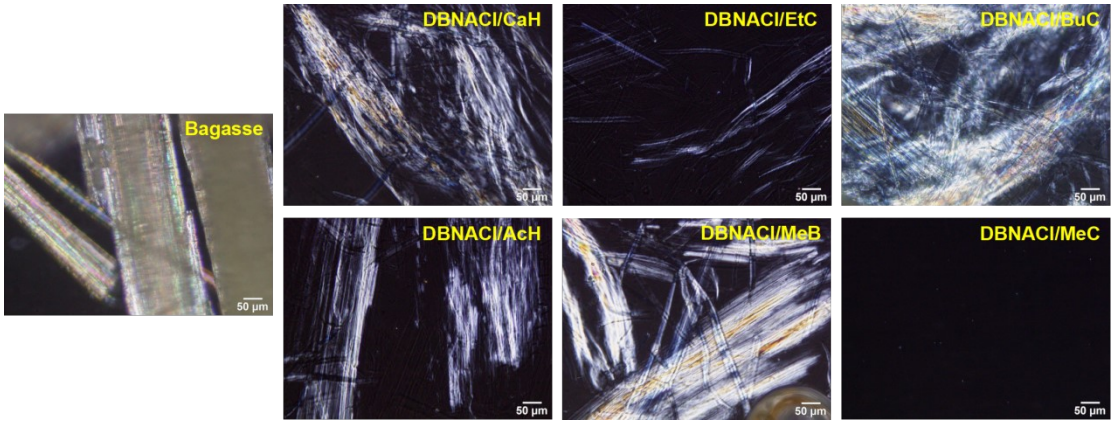

Fig. S6. PLM images of bagasse in various solvents.

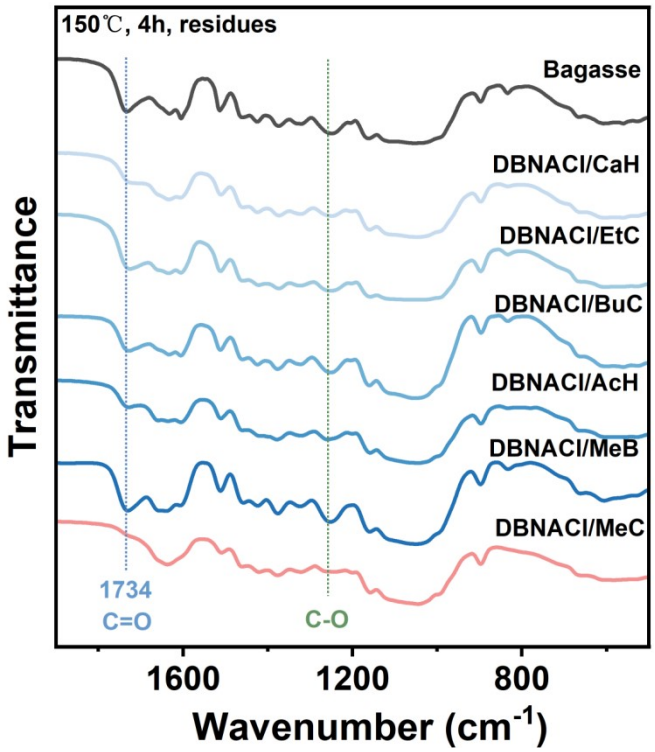

Fig. S7. FTIR spectra of bagasse in various solvents.

Table S2. Regeneration rate and component analysis of the bagasse after dissolution.

Samples	Regeneration rate (%)	Component content (%)		
		cellulose	hemicellulose	lignin
Bagasse	100	49.5	25.3	23.5
DBNACl-bagasse	28.8	21.2	5.1	73.6
DBNACl/MeC-bagasse	68.4	70.7	8.9	20.3

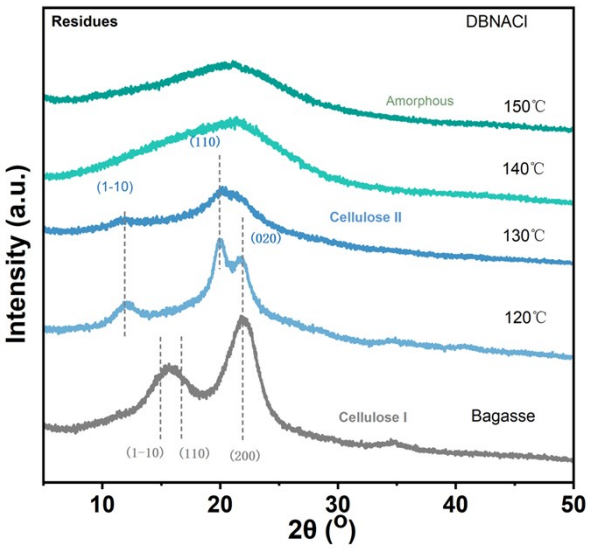

Fig. S8. XRD patterns of regenerated bagasse under different treatment temperature in DBNACl system.

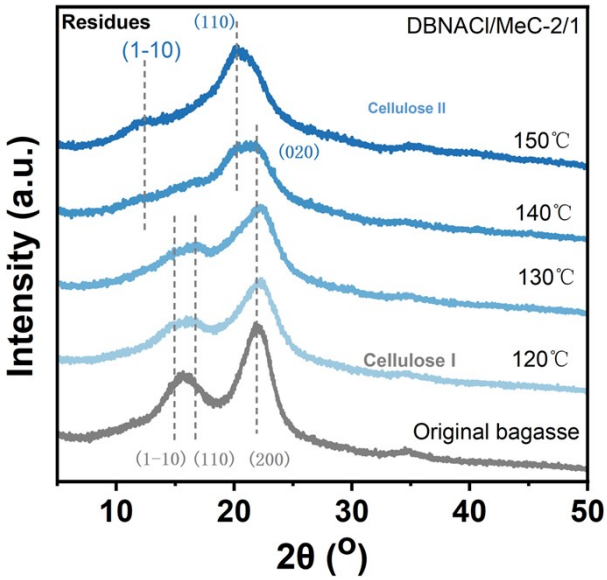

Fig. S9. XRD patterns of regenerated bagasse under different treatment temperature in DBNACl/MeC-2/1 system.

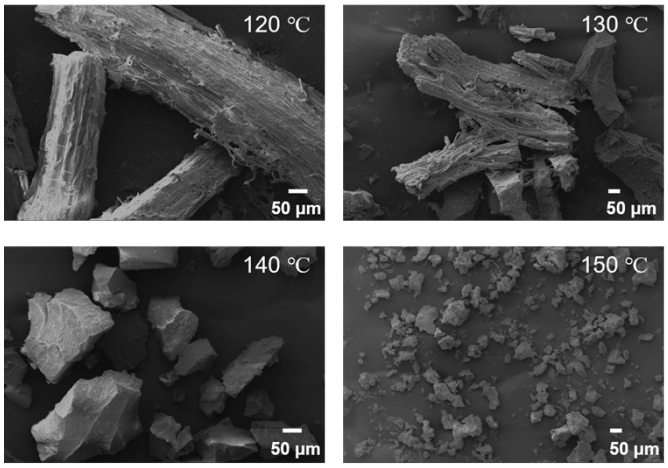

Fig. S10. SEM images of regenerated bagasse under different treatment temperature in DBNACl system.

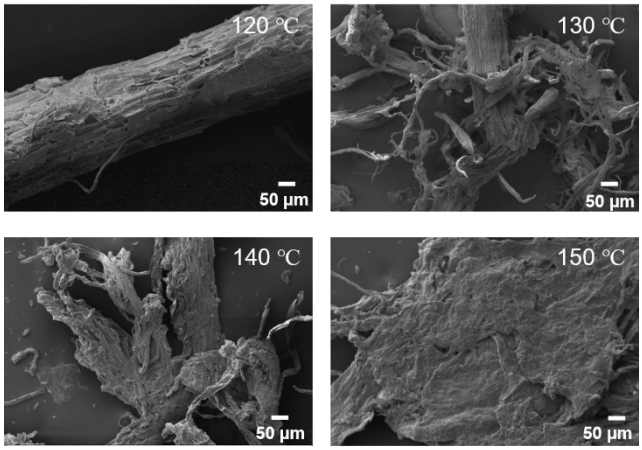

Fig. S11. SEM images of regenerated bagasse under different treatment temperature in DBNACl/MeC-2/1 system.

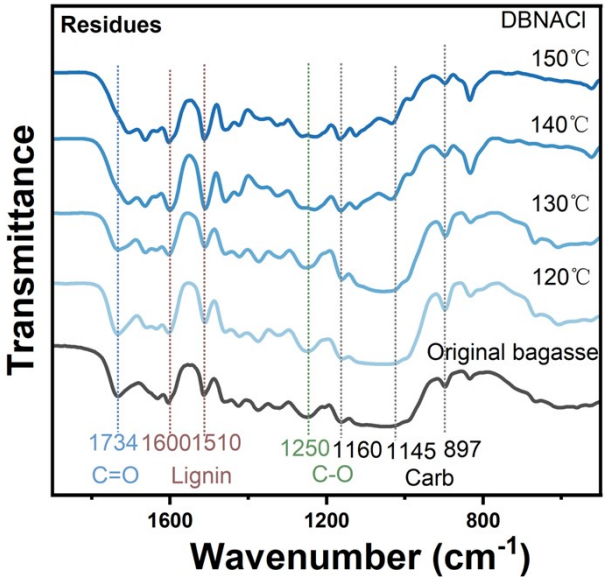

Fig. S12. FTIR spectra of regenerated bagasse under different treatment temperature in DBNACl system.

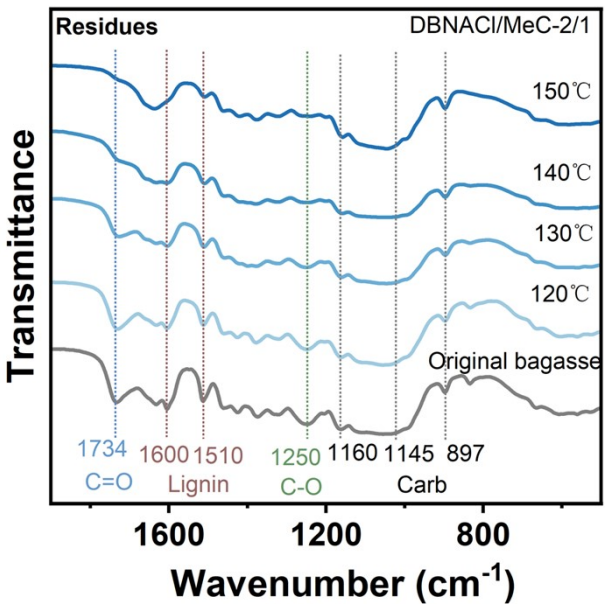

Fig. S13. FTIR spectra of regenerated bagasse under different treatment temperature in DBNACl/MeC-2/1 system.

Table S3. C/O ratio and relative content of C1s on the surface of regenerated bagasse.

Samples	C/O	C1s content (%)			
		C1	C2	C3	C4
Bagasse	3.69	70.45	17.59	4.56	7.30
DBNACl-bagasse	6.55	82.82	13.16	0.83	3.19
DBNACl/MeC-bagasse	1.77	33.83	57.00	5.54	3.63

Table S4. Semi-quantitative analysis of lignin units and linkages (per 100 aromatic rings).

Structural unit /connection bond	MBL	DBNACl-L	DBNACl/MeC-L
S	50.9	68.3	57.3
G	44.2	29.2	36.3
H	5.0	2.4	6.4
S/G	1.15	2.35	1.58
pCA+FA	30.8	45.1	5.5
β-O-4	51.4	22.5	46.1
β-β	3.8	0	3.6
β-5	3.0	0	2.8

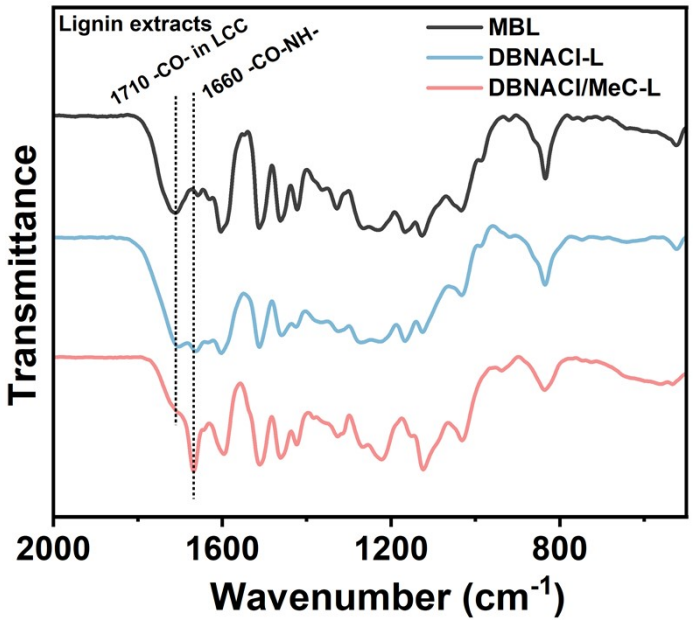

Fig. S14. FITR spectra of lignin.

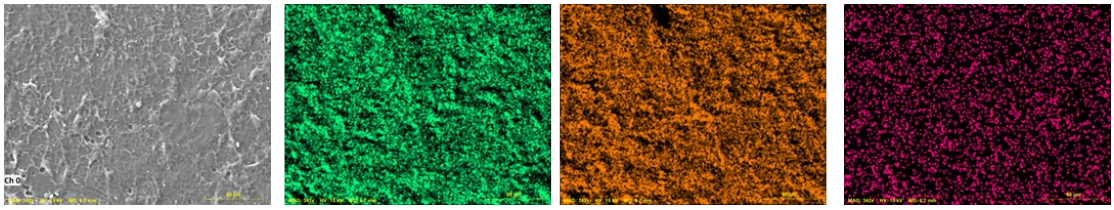

Fig. S15. SEM image of bagasse film from DBNACl/MeC.

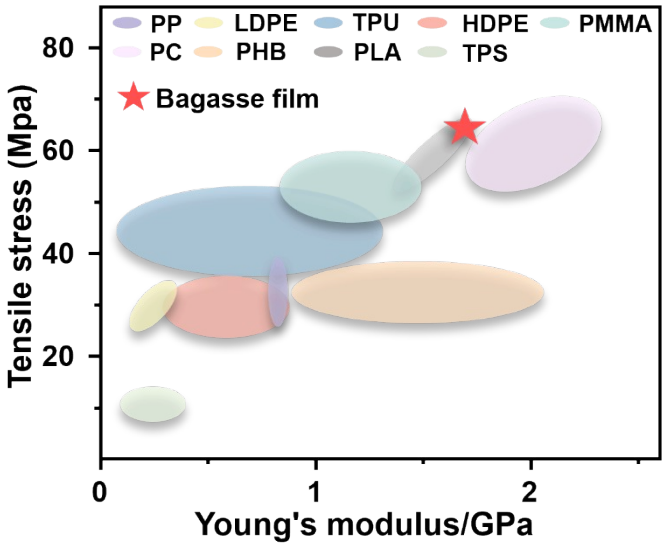

Fig. S16. Comparison of mechanical properties for bagasse film with other materials.

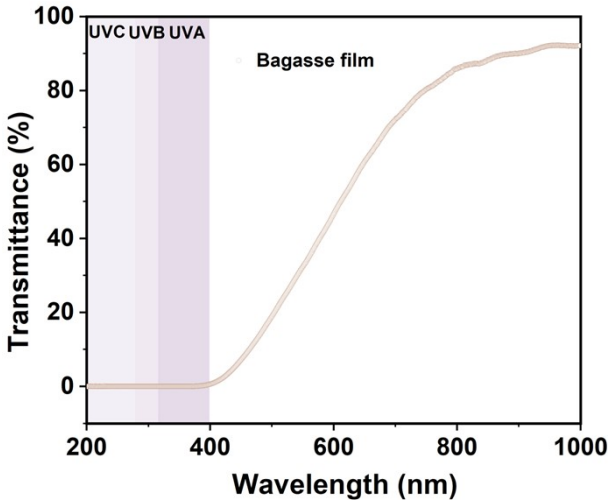

Fig. S17. Transmittance curve of bagasse film.

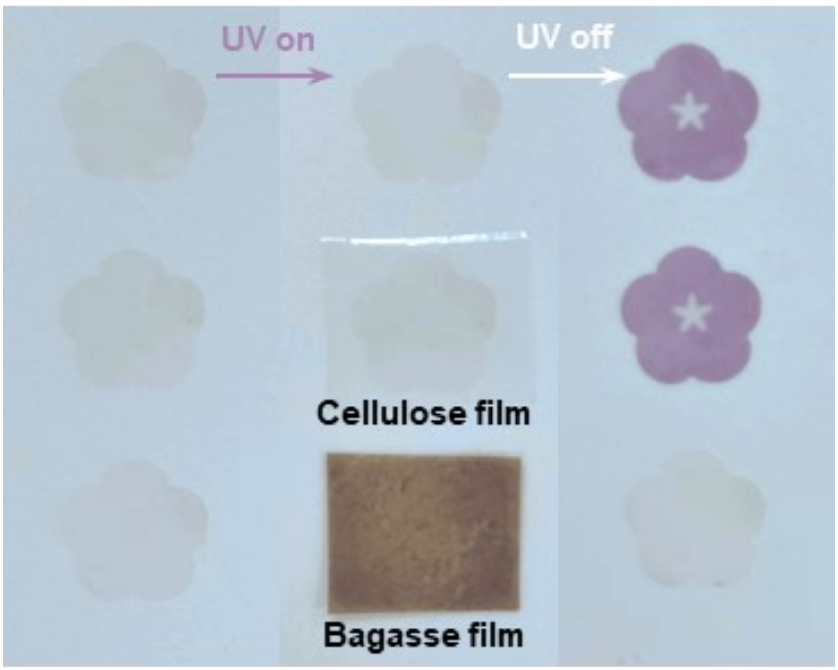

Fig. S18. UV resistance of bagasse film.

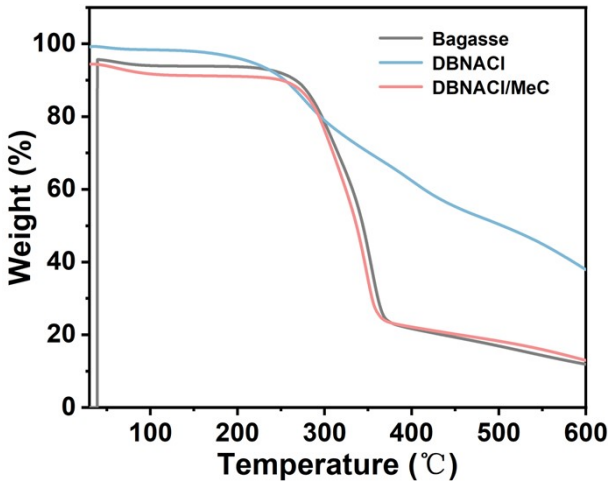

Fig. S19. TGA curve of films.

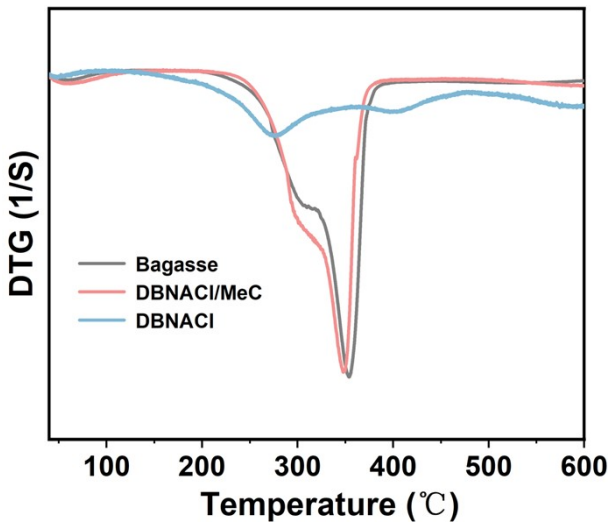

Fig. S20. DTG curves of films.

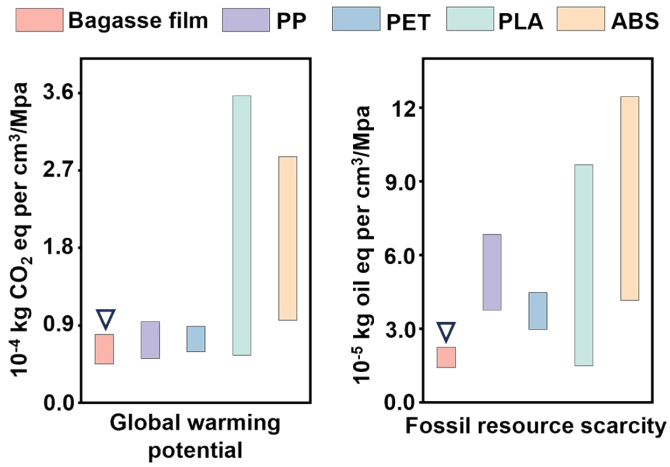

Fig. S21. Life cycle assessment of bagasse film compared to those of PP, PET, PLA, and ABS, respectively.

Table S5. Mechanical properties of composite bagasse materials

Sample	Tensile stress (MPa)	Tensile strain (%)	Young's modulus (GPa)
Regenerated bagasse film	64.5±5.30	5.5±1.50	1.76±0.20
A4 paper	12.6±1.67	3.36±0.31	1.12±0.0049
Regenerated bagasse composite paper	25.25±1.29	4.08±0.14	0.80±0.012
Balshawood slices-X	0.60±0.10	4.79±0.30	0.034±0.000020
Regenerated bagasse composite wood chips-X	11.52±4.38	2.92±2.47	2.05±0.20
Balshawood slices-Y	18.61±1.93	1.35±0.10	2.08±0.26
Regenerated bagasse composite wood chips-Y	74.57±2.08	1.35±0.12	6.94±0.020

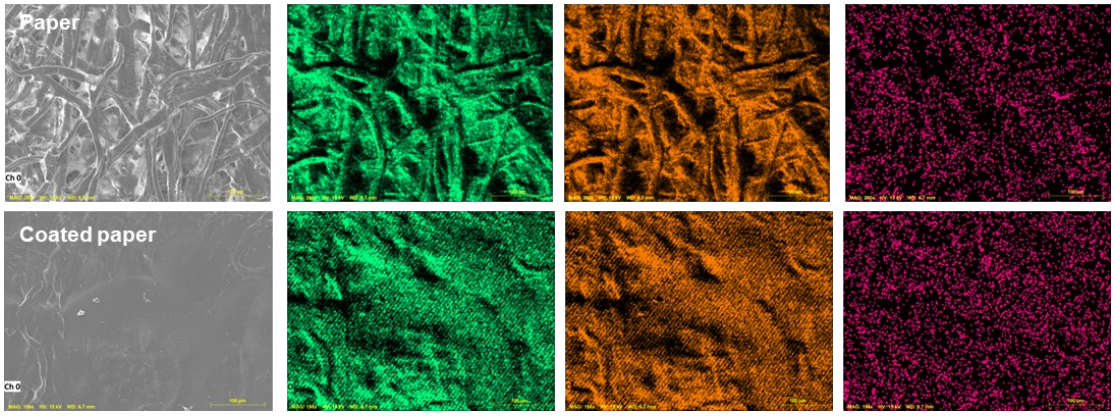

Fig. S22. SEM images of paper and coated paper.